Ren *et al. Micro and Nano Syst Lett (2017) 5:13*
DOI 10.1186/s40486-017-0048-8

Micro and Nano Systems Letters

LETTER Open Access

Effect of temperature on a miniaturized microbial fuel cell (MFC)

Hao Ren*, Chenming Jiang and Junseok Chae

Abstract

A microbial fuel cell (MFC) is a bioinspired energy converter which directly converts biomass into electricity through the catalytic activity of a specific species of bacteria. The effect of temperature on a miniaturized microbial fuel cell with *Geobacter sulfurreducens* dominated mixed inoculum is investigated in this paper for the first time. The miniaturized MFC warrants investigation due to its small thermal mass, and a customized setup is built for the temperature effect characterization. The experiment demonstrates that the optimal temperature for the miniaturized MFC is 322–326 K (49–53 °C). When the temperature is increased from 294 to 322 K, a remarkable current density improvement of 282% is observed, from 2.2 to 6.2 Am^{-2}. Furthermore, we perform in depth analysis on the effect of temperature on the miniaturized MFC, and found that the activation energy for the current limiting mechanism of the MFC is approximately between 0.132 and 0.146 eV, and the result suggest that the electron transfer between *cytochrome* c is the limiting process for the miniaturized MFC.

Keywords: Microbial fuel cell (MFC), Micro-electro-mechanical systems (MEMS), Temperature effect, Activation energy, Extracellular electron transfer (EET), Cytochrome c, Rate limiting step

Background

A microbial fuel cell electrochemically converts biomass into electricity through the catalytic activity of specific species of bacteria, named exoelectrogen or anode-respiring bacteria, which are capable of transfer electrons outside their outer membrane [1–3]. During the past two decades, significant improvement on MFC has been demonstrated; for instance, the power density of microbial fuel cells have improved by more than four orders of magnitude, from 0.1 mWm^{-2} to 7.72 Wm^{-2} [4–6]. In order to improve the power density, a number of research have been performed, such as implementing the anode with high surface area to volume ratio [5, 7–9], investigating the performance of different species of exoelectrogen [10, 11], investigating different MFC configurations, and investigating different operation conditions, including temperature, pH, flow rate, etc. [12–15]. The two most investigated exoelectrogen are *Shewanella* and *Geobacter*, which generally generate higher current and power density than other types of exoelectrogen. The effect of temperature on microbial fuel cells with *Geobacter* as exoelectrogen has been investigated by many researchers, and it is reported that the optimal temperature to be 298–303 K (25–30 °C) for macro/mesoscale MFCs [13, 15].

Miniaturized MFCs are emerging technologies that utilize microfabrication for MFCs, which results in the characteristics of small footprint, low expense, batch fabrication, improved diffusion, high surface area to volume to ratio, etc. [1, 16–18]. Particularly, the small footprint makes miniaturized MFCs with a very small thermal mass, which is suitable for the temperature to be controlled within a short period of time [19]. We perform first-order calculation and found that the miniaturized MFC can be heated to the target temperature within several minutes due to its low heat capacity, which is suitable for characterizing the effect of temperature on MFCs, while macroscale MFCs takes much longer time (supporting materials). We have demonstrated miniaturized MFCs and microbial supercapacitors with record power densities of 1.12×10^4 and 3.95×10^5 Wm^{-3}; yet the effect of temperature on miniaturized MFCs haven't been

*Correspondence: hren12@asu.edu
School of Electrical, Computer and Energy Engineering, Arizona State University, Tempe, AZ, USA

studied to date [5, 7, 20]. In this paper, we report the first study of temperature effect on a miniaturized MFC with *Geobacter* dominated mixed species. Our results show that the miniaturized MFC has an optimal temperature at 322–326 K.

Methods

A customized setup including a miniaturized microbial fuel cell (MFC) with an anode chamber of 50 µL and a close-loop temperature controlled oven was built, as illustrated in Fig. 1. The process flow for the miniaturized MFC fabrication is illustrated in Fig. 1a. The miniaturized MFC had a proton exchange membrane (PEM) (Nafion 117, Sigma Aldrich), to permit cation transport and to avoid electrical short-circuiting and electrolyte cross mixing. Two silicone gaskets with thicknesses of 500 µm were sandwiched between two glass slides. Ti/Pt (20/100 nm) was deposited by electron beam evaporation for both glass slides in order to form anode and cathode. The volume of each chamber was 50 µL, and the size of electrode was 1 cm^2. Two nanoports (10–32 Coned assembly, IDEX Health and Science) were used to provide microfluidic pathways into and out of each chamber. The MFC was assembled with four screw bolts and nuts to minimize oxygen/electrolyte leakage. An optical image of the miniaturized MFC after assembly is depicted in Fig. 1b.

The inoculum for the MFC reactor was obtained from an acetate-fed microbial electrolysis cell (MEC) that had *Geobacter*-enriched bacterial community originally from anaerobic-digestion sludge. Clone libraries of the 16S-rRNA gene showed that the inoculum was a mixed bacterial culture dominated by *Geobacter sulfurreducens*. The anolyte was 25-mM sodium acetate medium with 1680 mg KH_2PO_4, 12,400 mg Na_2HPO_4, 1600 mg NaCl, 380 mg NH_4Cl, 5 mg EDTA, 30 mg $MgSO_4{\cdot}7H_2O$, 5 mg $MnSO_4{\cdot}H_2O$, 10 mg NaCl, 1 mg $Co(NO_3)_2$, 1 mg $CaCl_2$, 0.001 mg $ZnSO_4{\cdot}7H_2O$, 0.001 mg $ZnSO_4{\cdot}7H_2O$, 0.1 mg $CuSO_4{\cdot}5H_2O$, 0.1 mg $AlK(SO_4)_2$, 0.1 mg H_3BO_3, 0.1 mg $Na_2MoO_4{\cdot}2H_2O$, 0.1 mg Na_2SeO_3, 0.1 mg $Na_2WO_4{\cdot}2H_2O$, 0.2 mg $NiCl_2{\cdot}6H_2O$, and 1 mg $FeSO_4{\cdot}7H_2O$ (per liter of deionized water) (pH 7.8 ± 0.2). For the start-up process, inoculum and anolyte were mixed with a volume ratio of 1:1. The catholyte was 100-mM potassium ferricyanide in 100-mM phosphate buffer solution (pH 7.4). A gravity convection oven was utilized to control the temperature of the MFC (Lindberg Blue M), as illustrated in Fig. 1c. The temperature of the oven was then controlled digitally with a resolution of 0.1 °C and was calibrated with a lab red spirit-filled precision thermometer. The current was

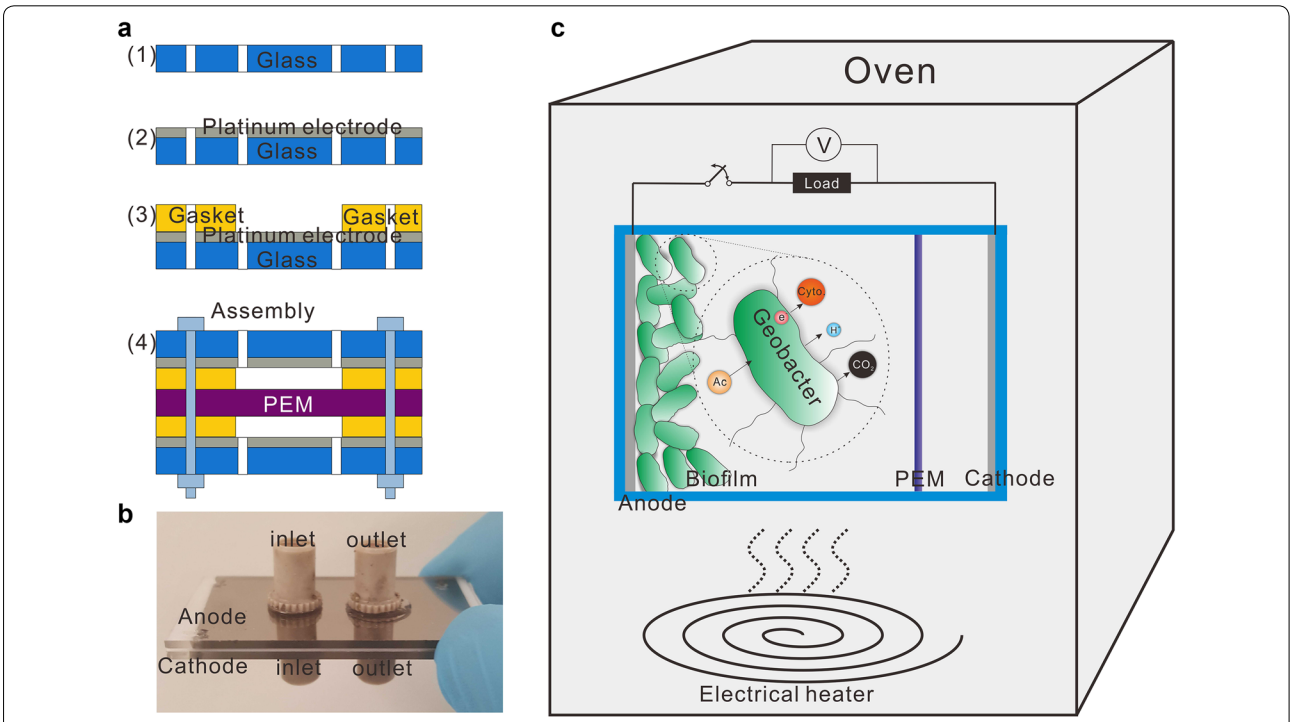

Fig. 1 A miniaturized microbial fuel cell (MFC) for the characterization of temperature effect: **a** fabrication process flow for the miniaturized MFC; **b** Optical image of the miniaturized MFC after assembly; **c** illustration of the miniaturized MFC mounted inside a gravity convection oven with close-loop temperature control. The miniaturized MFC has a chamber volume of merely 50 µL, allowing the temperature inside the MFC to be controlled by the oven due to its small thermal mass

monitored by recording the voltage drop across an external resistor connected between the anode and the cathode using a data acquisition system (DAQ/68, National Instrument). At least three replicates were conducted for all experiments.

Due to its small thermal mass, the miniaturized MFC allowed the temperature inside anode chamber of the MFC to match well with the ambient temperature in the oven. The start-up processes of the miniaturized MFCs in elevated temperature of 314 K and at a room temperature of 294 K and elevated temperature of 314 K are shown in Additional file 1: Figures S1 and S2, respectively.

Results

First, we characterized the impact of the temperature on the performance of the miniaturized MFC when a thick biofilm is formed on top, and the biofilm is grown at a temperature of 314 K. The temperature was changed periodically from 294 to 332 K with six intervals. For each temperature, we waited three to 6 h for the current became stable. As shown in Fig. 2, the current density first increased with the increase of temperature, and then decreased. At a temperature of 294 K, a power density of mere 2.2 Am^{-2} was obtained while at a temperature of 322 K, the highest current density of 6.2 Am^{-2} was reached. The reason for the drop of current density was believed to be that the high temperature made the *Geobacter* less active.

Analyzing Fig. 2, the increase of the current comes from two parts: (1) at high temperature, the output current for exoelectrogen increases; (2) at high temperature, the number of exoelectrogen which become active also increases. A second experiment was performed on the miniaturized MFC during its start-up process under a temperature of 294 K, and the temperature was controlled by the oven ranging from 294 to 325 K (the maximum temperature is kept at 325 K so that the device will not fail due to high temperature). For each temperature, a period of 5–7 min was kept until increasing the temperature. The short time prevent the exoelectrogen from proliferating since there is not enough time. Therefore, we can assume that the amount of exoelectrogen is kept constant during the temperature adjustment phase. The result of the current density versus temperature is shown in Fig. 3. The current increases with the temperature, which is in similar trend with Fig. 2. As a result, it also shows that the temperature has a direct impact on the current output of the MFC.

Discussion

We try to perform more in depth analysis on the temperature effect on the miniaturized MFC result. Firstly, we try to derive equation about the relationship between the output current versus the temperature.

According to the Marcus theory, the rate constant for electron transfer is expressed as [21]:

$$\begin{aligned} k_{et} &= \frac{2\pi}{\hbar} H_{AB}^2 \frac{1}{\sqrt{4\pi k_b T}} \exp\left(-\frac{(\lambda + \Delta G^\circ)^2}{4\lambda k_b T}\right) \\ &= \frac{2\pi}{\hbar} H_{AB}^2 \frac{1}{\sqrt{4\pi k_b T}} \exp\left(-\frac{\Delta G^\dagger}{k_b T}\right) \end{aligned} \quad (1)$$

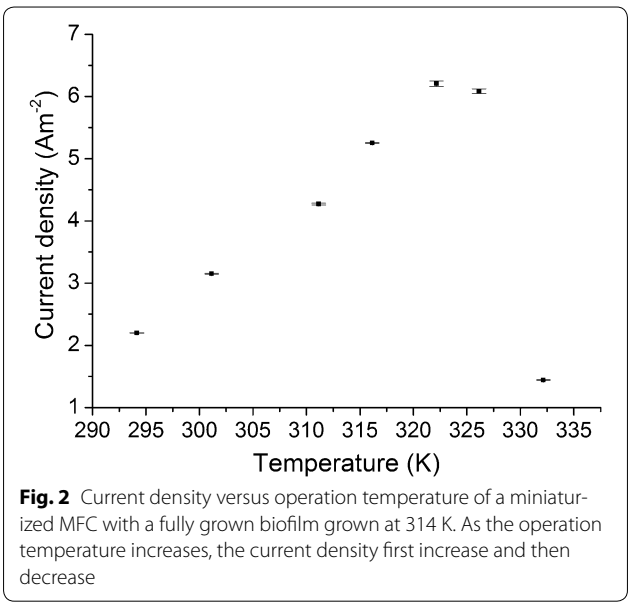

Fig. 2 Current density versus operation temperature of a miniaturized MFC with a fully grown biofilm grown at 314 K. As the operation temperature increases, the current density first increase and then decrease

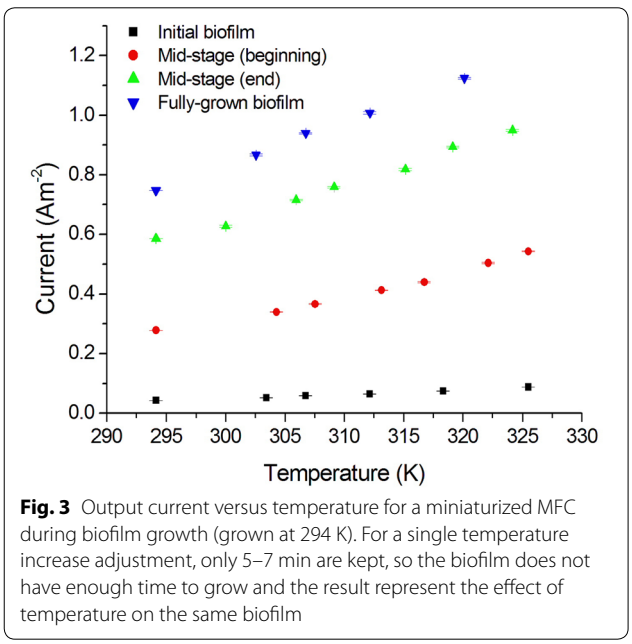

Fig. 3 Output current versus temperature for a miniaturized MFC during biofilm growth (grown at 294 K). For a single temperature increase adjustment, only 5–7 min are kept, so the biofilm does not have enough time to grow and the result represent the effect of temperature on the same biofilm

where k_{et} is the rate constant of the rate-limiting step in catalytic activity of *G. sulfurreducens*, H_{AB} is the electron coupling between initial and final state, λ is the reorganization energy, $\hbar$ is the reduced Planck constant, $\Delta G°$ is the total Gibbs energy change during the electron transfer, k_b is the Boltzmann constant, T is the absolute temperature, and $\Delta G^{\dagger}$ is the activation energy associated with a rate-limiting step in catalytic activity of *G. sulfurreducens*, where

$$\Delta G^{\dagger} = \frac{(\lambda + \Delta G°)^2}{4\lambda}$$

As a result, assuming the rate-limiting step is a first order reaction, the current in the catalytic activity of *G. sulfurreducens* can be written as

$$I = C \cdot k_{et} \cdot M = \frac{2\pi}{\hbar} C \cdot H_{AB}^2 \frac{1}{\sqrt{4\pi k_b T}} \exp\left(-\frac{\Delta G^{\dagger}}{k_b T}\right) \cdot M \tag{2}$$

Here C is a constant for the reaction. Rearranging Eq. 2 results in

$$\ln\left(I \cdot \sqrt{T}\right) = \ln\left(\frac{2\pi}{\hbar} C \cdot H_{AB}^2 \frac{1}{\sqrt{4\pi k_b}} M\right) - \frac{\Delta G^{\dagger}}{k_b T} \tag{3}$$

Equation 3 shows a linear relationship between the $\ln(I{\cdot}T^{0.5})$ and T^{-1} and the slope is $-\Delta G^{\dagger}/k_b$. As a result, by linearly fitting the curve of $\ln(I{\cdot}T^{0.5})$ versus T^{-1}, the activation energy of the rate-limiting step in EET is obtained.

$Ln(I{\cdot}T^{0.5})$ and T^{-1} curve for biofilm during the start-up process with different steady-state current at 294 K, ranging from 0.04 to 0.84 Am^{-2} is plotted based on Fig. 3, as shown in Fig. 4, where the 0.04 Am^{-2} represent very initial biofilm, while the 0.84 Am^{-2} represent fully grown biofilm. According to Fig. 4a, a linear relationship between $ln(I{\cdot}T^{0.5})$ and T^{-1} is found for all four curves, and linearly fitting the curves in Fig. 4a results in the corresponding activation energies. As the activation energy shows, in the very initial biofilm and mid-stage (beginning) biofilm, the activation energy ranges from 0.189 to 0.202 eV. For mid-stage (end) biofilm to fully grown biofilm, the activation energy drops to 0.132–0.146 eV.

We also plot the $ln(I{\cdot}T^{0.5})$ versus T^{-1} curve based on the data for Fig. 2, as shown in Fig. 5.

A linear relationship between $ln(I{\cdot}T^{0.5})$ and T^{-1} is also found for the fully grown biofilm; however, the slope in Fig. 5a is much larger than Fig. 4a. The reason for this phenomenon is that as temperature increases, not only does the rate constant, k_{et} increase, but also the amount of redox cofactors, M_{red} increases exponentially based on in Eq. 3. Thus because we use the same miniaturized MFC setup and the same inoculum to obtain Figs. 4 and 5, we can assume the k_{et} for fully grown biofilm is the same as Fig. 4 for fully grown biofilm, 0.132 eV. Therefore, we can calculate the change in amount of redox cofactor contributing to the EET as temperature changes, as shown in Fig. 5b, which shows a linear relationship between $\ln(M_{red})$ and T^{-1}. Linearly fitting the curve also results in an activation energy of 0.155 eV.

The activation energy in the rate-limiting step of catalytic activity of *G. sulfurreducens* is compared with activation energies of individual catalytic activity of *G. sulfurreducens* steps, as shown in Table 1. It is found that the activation energy of this work fits very well to the electron transfer between *cytochrome* c, while being very far from activation energies of other steps associated with EET. This suggests that the rate-limiting step is the *cytochrome* c.

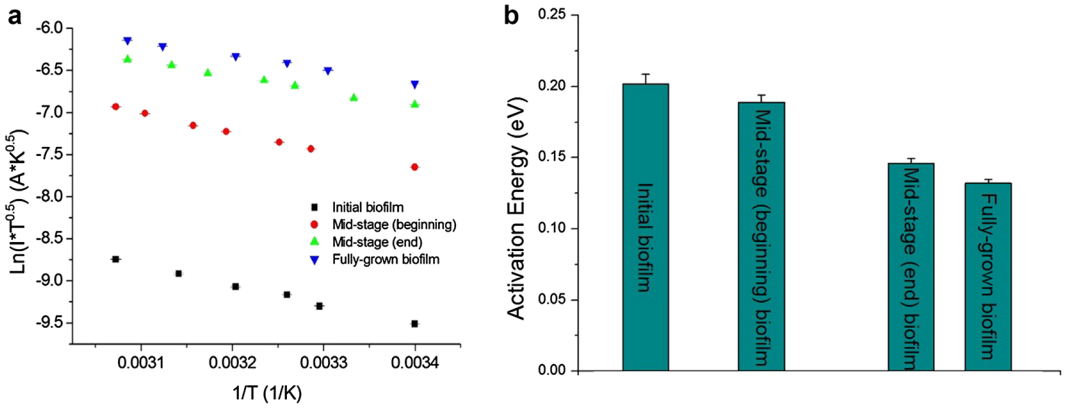

Fig. 4 **a** $\ln(I{\cdot}T^{0.5})$ and T^{-1} curve for biofilm at biofilm formation stages with different maximum steady state current densities during the start-up process, linear relationships are observed for all curves, and activation energy are obtained through Eq. 3, as shown in **b**

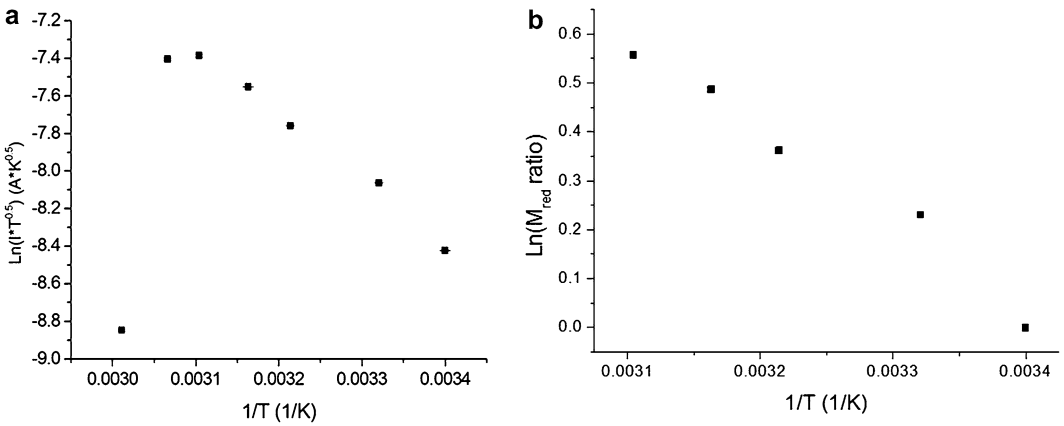

Fig. 5 **a** $\ln(I \cdot T^{0.5})$ and T^{-1} curve for thick fully-grown biofilm grown at 314 K; **b** logarithmic amount of redox cofactors contributing to the steady-state current generation as temperature changes during fully grown biofilm by assuming the activation energy is 0.132 eV based on Fig. 4b; as temperature increases, a larger amount of redox cofactors are responsible for the catalytic activity of *Geobacter sulfurreducens*, suggesting that the catalytic activity of *Geobacter sulfurreducens* is temperature dependent and is favored by higher temperature

Table 1 the activation energy of the rate-limiting step of this work is compared with the activation energy reported by prior studies of the reactions related to EET

Reaction	Activation energy (eV)
Rate-limiting step of EET in this work	0.132–0.146
Cytochrome C electron transfer	0.14 ± 0.03 [22, 23]
Quinones reduction	0.477 [24]
Reduction of CoQ by NADH	0.86–1.23 [25]
Ubiquinol oxidation by the bc1 complex	0.466–0.518 [26]
Quinol oxidation	0.466 [27]
Iron-sulfur protein	0.02 [28]

It is found that the activation energy of this work is close to the electron transfer between cytochrome c, suggesting that the rate limiting step is the cytochrome c, especially for a thick biofilm, the activation energy of this work matches very well with the activation energy of cytochrome c electron transfer

Moreover, the activation energy for the amount of M_{red} versus *1/T*, 0.155 eV, falls in the activation energy range of *cytochrome* c, which also supports that for thick biofilm, the electron transfer between *cytochrome* c is critical for electron transfer from *G. sulfurreducens* to the anode, i.e. EET [29].

These findings suggest that the rate-limiting step for catalytic activity of *G. sulfurreducens* is the EET, which has long been a focus for studies in microbial electrochemical technology (MET). The result is consistent with prior evidences. For instance, Liu and Bond [29] found that all *cytochrome c* proteins were oxidized at the initial biofilm formation stage, whereas reduced *cytochrome c* accumulated in thick biofilms, suggesting a part of the *cytochrome c* located far from the anode cannot transport their electrons to the anode. It suggests that the long range electron transfer is the limiting mechanism for EET. Strycharz-Graven et al. [30] observed cyclic voltammetry peaks at a slow scan rate and reported that EET driven by redox reaction is limited either by electron transfer from inside the exoelectrogen to the outside of the exoelectrogen or from outside the exoelectrogen to the anode. Bonanni et al. [31] performed numerical modeling on the EET found that electron transfer limited the respiration rate of the cells for biofilm far from the anode. Our result not only concurs existing findings, but also is the first findings to experimentally pinpoint that electron transport among *cytochrome* c is the rate-limiting mechanism for EET.

Furthermore, the activation energy for the amount of redox cofactors versus *1/T*, 0.155 eV, supports that electron transfer between *cytochrome* c is a critical step for EET. For thick biofilm, as temperature increases, the amount of *cytochrome* c contributing to EET also increases, suggesting that electron transfer between *cytochrome* c is the main long-range EET mechanism. This finding is in agreement with prior studies by Snider et al. [32] that long-range electron transport in *G. sulfurreducens* biofilms is driven by *cytochrome* c redox gradient. In the meantime, it is not contradictory with the findings that nano-pili secreted by *G. sulfurreducens* are conductive [31–35], as the nano-pili may not be the major electron transfer mechanism.

In addition, from our finding, miniaturized MFC performs better at an elevated temperature, which concurs with the trend of macro-sized MFCs [36]. This finding may help our future MFC design to seek for optimal temperature to be established.

Conclusion

A miniaturized MFC is built to characterize its current output capability as a function of the temperature. The result shows that the output current increases as temperature increases from 294 to 322 K, and an optimal temperature for the MFC is 322–326 K (49–53 °C), which indicates the thermal activation characteristic of the miniaturized MFC. Further in depth analysis reveals that the activation energy for the current limiting mechanism of the MFC is 0.132–0.146 eV, suggesting that the electron transfer between *cytochrome* c is the limiting process for the miniaturized MFC.

Additional file

Additional file 1. Supporting materials.

Authors' contributions

HR designed and fabricated the miniaturized microbial fuel cells, carried out experiments and analyzed the data. CJ supported fabrication, experiments and analysis the data. HR and JC conceived the project. All authors read and approved the final manuscript.

Competing interests

The authors declare that they have no competing interests.

Funding

The authors declare that they have no funding support to this research.

Received: 29 October 2016 Accepted: 3 February 2017
Published online: 22 February 2017

References

1. Ren H, Lee H-S, Chae J (2012) Miniaturizing microbial fuel cells for potential portable power sources: promises and challenges. Microfluid Nanofluid 13(3):353–381. doi:10.1007/s10404-012-0986-7
2. Logan BE, Hamelers B, Rozendal R, Schröder U, Keller J, Freguia S, Aelterman P, Verstraete W, Rabaey K (2006) Microbial fuel cells: methodology and technology. Environ Sci Technol 40(17):5181–5192
3. Lovley DR (2008) Extracellular electron transfer: wires, capacitors, iron lungs, and more. Geobiology 6(3):225–231
4. Debabov V (2008) Electricity from microorganisms. Microbiology 77(2):123–131
5. Ren H, Tian H, Gardner CL, Ren T-L, Chae J (2016) A miniaturized microbial fuel cell with three-dimensional graphene macroporous scaffold anode demonstrating a record power density of over 10000 W m^{-3}. Nanoscale 8(6):3539–3547
6. Ren H, Rangaswami S, Lee H-S, Chae J (2016) Enhanced current and power density of micro-scale microbial fuel cells with ultramicroelectrode anodes. J Micromech Microeng 26(9):095016
7. Ren H, Pyo S, Lee J-I, Park T-J, Gittleson FS, Leung FC, Kim J, Taylor AD, Lee H-S, Chae J (2015) A high power density miniaturized microbial fuel cell having carbon nanotube anodes. J Power Sour 273:823–830
8. Chen SL, Hou HQ, Harnisch F, Patil SA, Carmona-Martinez AA, Agarwal S, Zhang YY, Sinha-Ray S, Yarin AL, Greiner A, Schroder U (2011) Electrospun and solution blown three-dimensional carbon fiber nonwovens for application as electrodes in microbial fuel cells. Energy Environ Sci 4(4):1417–1421. doi:10.1039/C0ee00446d
9. Xie X, Yu GH, Liu N, Bao ZN, Criddle CS, Cui Y (2012) Graphene-sponges as high-performance low-cost anodes for microbial fuel cells. Energy Environ Sci 5(5):6862–6866. doi:10.1039/C2ee03583a
10. Hou H, Li L, Cho Y, de Figueiredo P, Han A (2009) Microfabricated microbial fuel cell arrays reveal electrochemically active microbes. PLoS ONE 4(8):e6570
11. Choi G, Hassett DJ, Choi S (2015) A paper-based microbial fuel cell array for rapid and high-throughput screening of electricity-producing bacteria. Analyst 140(12):4277–4283
12. Abboud R, Popa R, Souza-Egipsy V, Giometti CS, Tollaksen S, Mosher JJ, Findlay RH, Nealson KH (2005) Low-temperature growth of *Shewanella oneidensis* MR-1. Appl Environ Microbiol 71(2): 811–816. http://aem.asm.org/content/71/2/811.abstract)
13. Cheng S, Xing D, Logan BE (2011) Electricity generation of single-chamber microbial fuel cells at low temperatures. Biosens Bioelectron 26(5):1913–1917
14. Liu H, Cheng S, Logan BE (2005) Power generation in fed-batch microbial fuel cells as a function of ionic strength, temperature, and reactor configuration. Environ Sci Technol 39(14):5488–5493
15. Min B, Román ÓB, Angelidaki I (2008) Importance of temperature and anodic medium composition on microbial fuel cell (MFC) performance. Biotechnol Lett 30(7):1213–1218
16. Jiang H, Halverson LJ, Dong L (2015) A miniature microbial fuel cell with conducting nanofibers-based 3D porous biofilm. J Micromech Microeng 25(12):125017
17. Choi S, Lee HS, Yang Y, Parameswaran P, Torres CI, Rittmann BE, Chae J (2011) A mu L-scale micromachined microbial fuel cell having high power density. Lab Chip 11(6):1110–1117. doi:10.1039/C0lc00494d
18. Chen W, Fang R, Balaban MB, Yu W, Gonzalez-Velo Y, Barnaby HJ, Kozicki MN (2016) A CMOS-compatible electronic synapse device based on Cu/SiO2/W programmable metallization cells. Nanotechnology 27(25):255202
19. Liu C (2012) Foundations of MEMS. Pearson Education Inc., Upper Saddle River, NJ
20. Ren H, Tian H, Lee H-S, Park T, Leung FC, Ren, T-L, Chae J (2015) Regulating the respiration of microbe: a bio-inspired high performance microbial supercapacitor with graphene based electrodes and its kinetic features. Nano Energy 15:697–708
21. Marcus RA (1993) Electron transfer reactions in chemistry: theory and experiment. Rev Mod Phys 65(3):599
22. Jortner J (1976) Temperature dependent activation energy for electron transfer between biological molecules. J Chem Phys 64(12):4860–4867
23. O'Reilly NJ, Magner E (2005) Electrochemistry of cytochrome c in aqueous and mixed solvent solutions: thermodynamics, kinetics, and the effect of solvent dielectric constant. Langmuir 21(3):1009–1014
24. Okamura M, Isaacson R, Feher G (1979) Spectroscopic and kinetic properties of the transient intermediate acceptor in reaction centers of *Rhodopseudomonas sphaeroides*. Biochim Biophys Acta (BBA) Bioenerg 546(3): 394–417
25. Fato R, Estornell E, Di Bernardo S, Pallotti F, Parenti Castelli G, Lenaz G (1996) Steady-state kinetics of the reduction of coenzyme Q analogs by complex I (NADH: ubiquinone oxidoreductase) in bovine heart mitochondria and submitochondrial particles. Biochemistry 35(8):2705–2716
26. Crofts AR, Barquera B, Gennis RB, Kuras R, Guergova-Kuras M, Berry EA (1999) Mechanism of ubiquinol oxidation by the bc 1 complex: different domains of the quinol binding pocket and their role in the mechanism and binding of inhibitors. Biochemistry 38(48):15807–15826
27. Hong S, Ugulava N, Guergova-Kuras M, Crofts AR (1999) The energy landscape for ubihydroquinone oxidation at the Qo site of the bc 1 complex in *Rhodobacter sphaeroides*. J Biol Chem 274(48):33931–33944
28. Dolan EA (2003) Theoretical studies of iron-sulfur electron transfer proteins. Washington State University, Washington
29. Liu Y, Bond DR (2012) Long-distance electron transfer by *G. sulfurreducens* biofilms results in accumulation of reduced c-type cytochromes. ChemSusChem 5(6):1047–1053
30. Strycharz-Glaven SM, Tender LM (2012) Study of the mechanism of catalytic activity of *G. sulfurreducens* biofilm anodes during biofilm growth. ChemSusChem 5(6):1106–1118
31. Bonanni PS, Bradley DF, Schrott GD, Busalmen JP (2013) Limitations for current production in *Geobacter sulfurreducens* biofilms. ChemSusChem 6(4):711–720
32. Snider RM, Strycharz-Glaven SM, Tsoi SD, Erickson JS, Tender LM (2012) Long-range electron transport in *Geobacter sulfurreducens* biofilms is redox gradient-driven. P Natl Acad Sci USA 109(38):15467–15472. doi:10.1073/pnas.1209829109

33. Reguera G, McCarthy KD, Mehta T, Nicoll JS, Tuominen MT, Lovley DR (2005) Extracellular electron transfer via microbial nanowires. Nature 435(7045):1098–1101
34. Malvankar NS, Vargas M, Nevin KP, Franks AE, Leang C, Kim BC, Inoue K, Mester T, Covalla SF, Johnson JP, Rotello VM, Tuominen MT, Lovley DR (2011) Tunable metallic-like conductivity in microbial nanowire networks. Nat Nanotechnol 6(9):573–579. doi:10.1038/Nnano.2011.119
35. Malvankar NS, Yalcin SE, Tuominen MT, Lovley DR (2014) Visualization of charge propagation along individual pili proteins using ambient electrostatic force microscopy. Nat Nanotechnol 9(12):1012–1017
36. del Campo AG, Lobato J, Cañizares P, Rodrigo M, Morales FF (2013) Short-term effects of temperature and COD in a microbial fuel cell. Appl Energy 101:213–217